Electronic Supplementary Material (ESI) for Journal of Materials Chemistry A.

Controlling phase separation in thermoelectric $Pb_{1-x}Ge_xTe$ to minimize thermal conductivity

Hong Lian,* Anil Kumar,[1] Václav Ocelík, Jacob Baas, Jamo Momand, Bart J. Kooi, and Graeme R. Blake*

Zernike Institute for Advanced Materials, University of Groningen, Nijenborgh 4, 9747 AG Groningen, The Netherlands

[1]Present address: Malvern Panalytical B.V., Lelyweg 1, 7602 EA Almelo, The Netherlands

Supplementary Material

Fig. S1. Additional SEM-BSE (backscattered electron) images of all five samples of $Pb_{0.51}Ge_{0.49}Te$ (see Fig. 1a for preparation conditions of each sample).

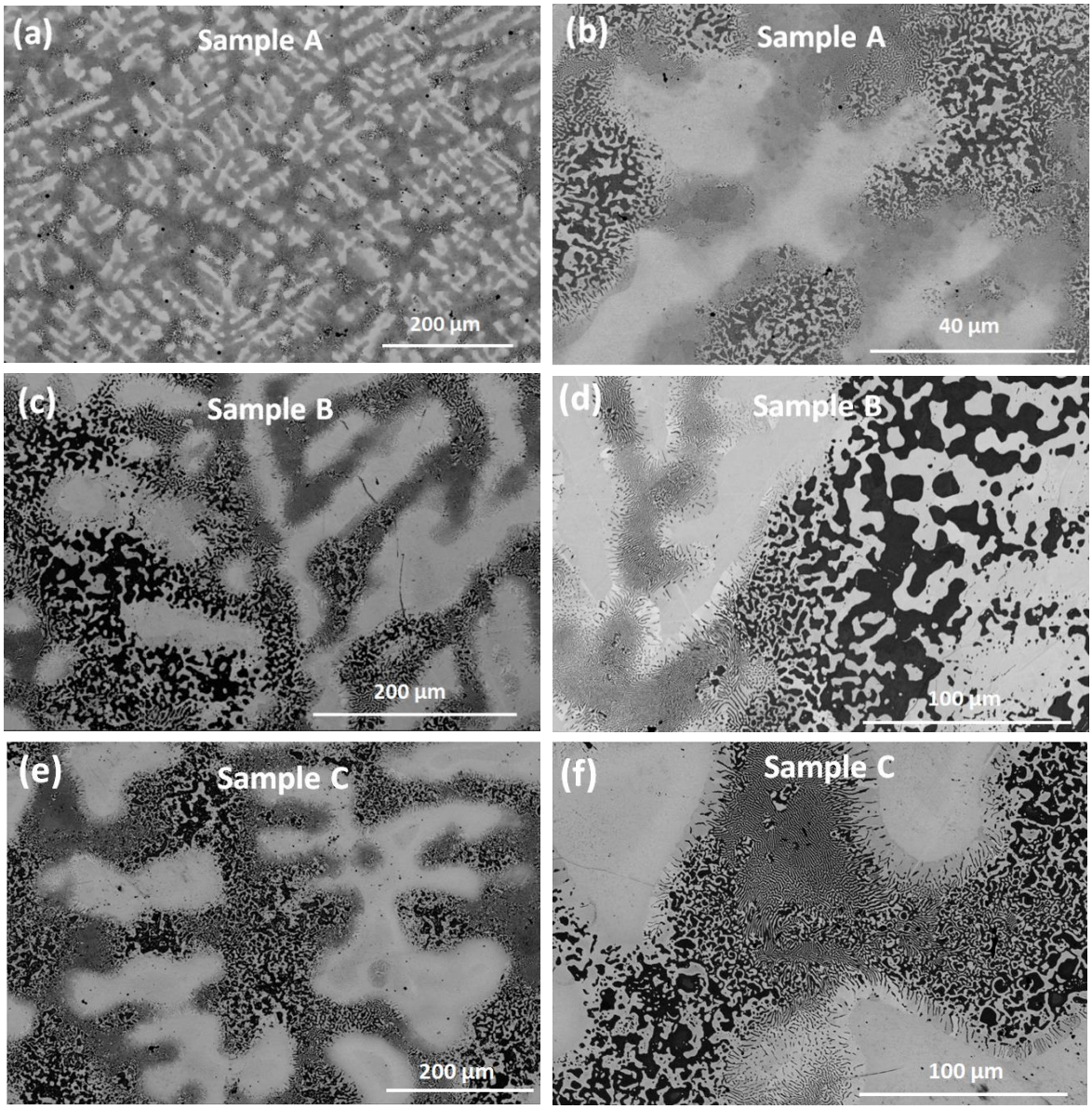

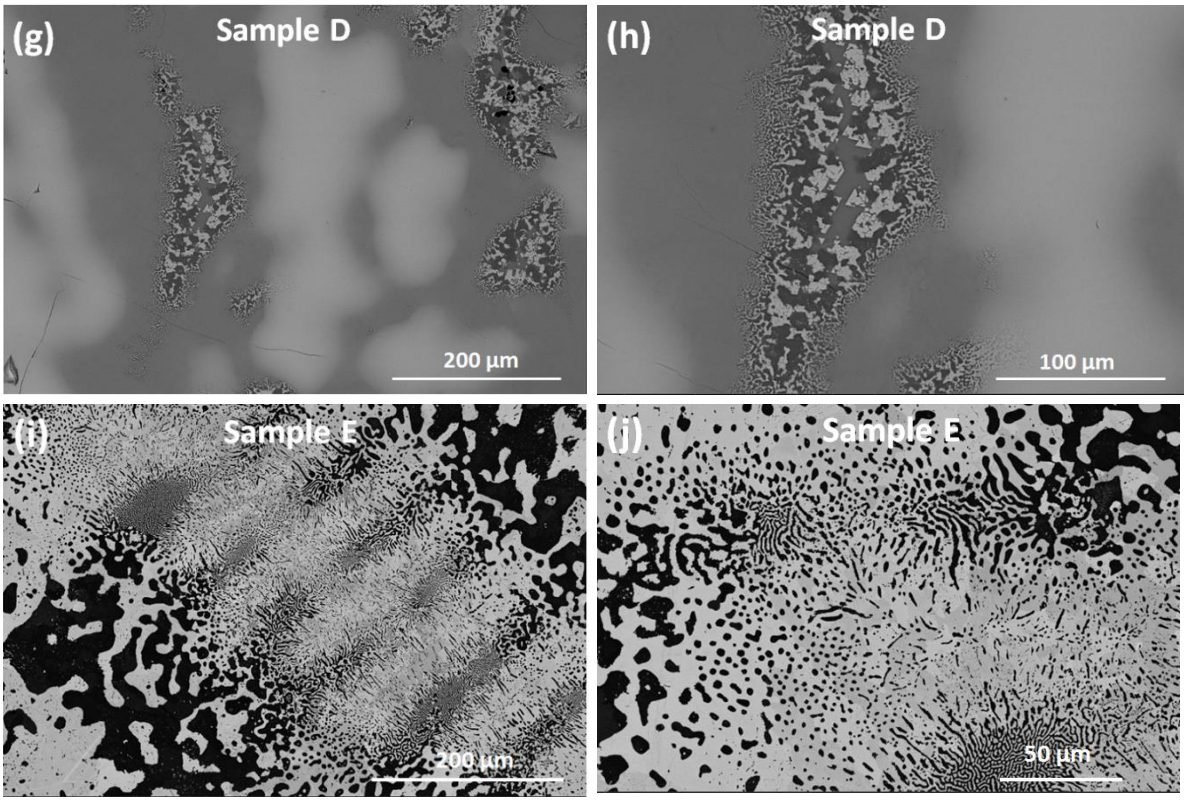
(g)
Sample D
200 µm
(h)
Sample D
100 µm
(i)
Sample E
200 µm
(j)
Sample E
50 µm

Fig. S2. Further SEM-BSE images of (a) sample B, (b) sample C, and (c) sample D. In each case the numerical labels indicate positions at which EDS spectra were measured (corresponding compositions are given in the tables). The as-prepared samples B-D represent intermediate cases of spinodal decomposition with respect to sample A (rapidly quenched to room temperature, slightly decomposed) and sample E (slow cooled, almost fully decomposed) discussed in the main text. Sample D is a unique case in that spinodal decomposition is close to complete, but a further tellurium-rich phase appears at the crystallographic grain boundaries [spot 5 in (c)].

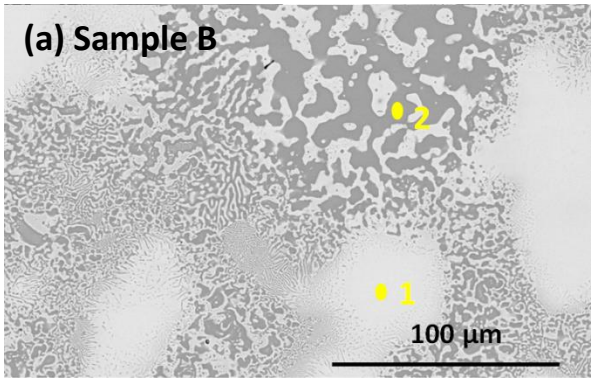

Element	Spot1 (at%)	Spot2 (at%)
TeL	46.7	49.7
GeK	7.3	46.1
PbL	46.0	4.2
Ge:Pb	14:86	91:9

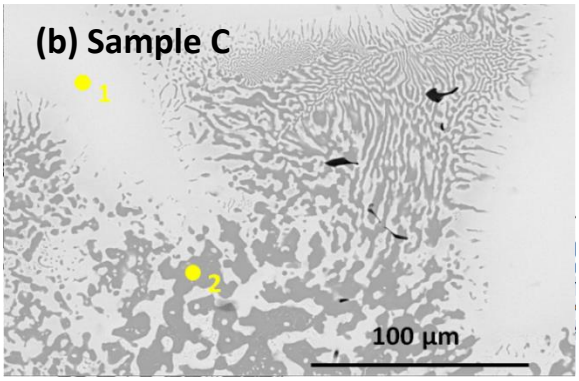

Element	Spot1 (at%)	Spot2 (at%)
TeL	47.1	49.1
GeK	10.5	44.9
PbL	42.4	6.0
Ge:Pb	19:81	88:12

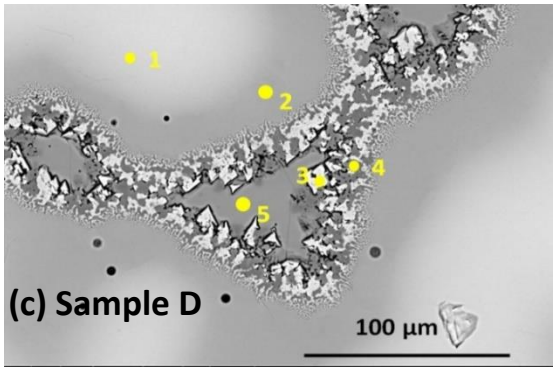

Ele-ment	Spot1 (at%)	Spot2 (at%)	Spot3 (at%)	Spot4 (at%)	Spot5 (at%)
TeL	46.4	47.8	47.2	48.7	78.5
GeK	10.4	31.2	8.3	46.0	17.2
PbL	43.2	21.0	44.5	5.3	4.3
Ge:Pb	19:81	59:41	15:85	89:11	81:19

Fig. S3. (a)-(d) Illustration of the process of using a focused ion beam to cut lamellae from sample A for TEM observation. (e) STEM image of part of a lamella extracted from an area of large-scale phase segregation. Ge-rich rhombohedral and Pb-rich cubic regions are apparent; the boundary is indicated by the dotted yellow line. Within the Ge-rich region a herringbone-like twin domain structure can be distinguished, typical for rocksalt-type structures with rhombohedral symmetry. A regular array of almost orthogonal domains can also be observed in the cubic Pb-rich region, with lengths of 50-400nm and widths of ~10nm. This might be due to the retention of a small amount of Ge in the PbTe phase; a chemical composition gradient is also suggested by the wide XRD peaks of the cubic phase.

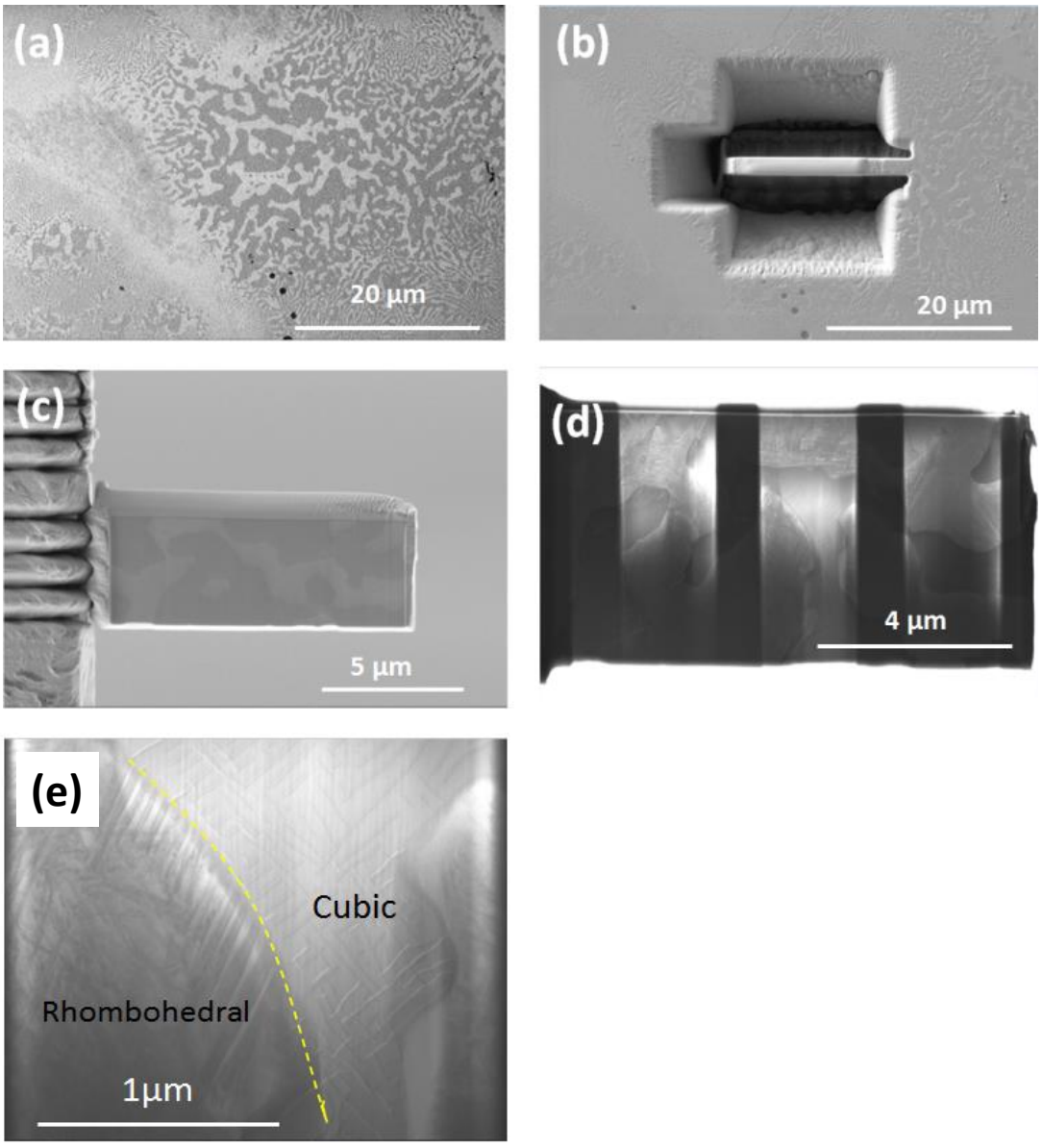

Fig. S4. Bright-field TEM images of lamellae 1, 3 and 4 taken from sample A (see Fig. 4 for the locations from which lamellae were extracted). Lamellae 3 and 4, taken from regions containing both Ge-rich and Pb-rich domains, exhibit complex microstructures / nanostructures with many defects in addition to chemically phase separated regions. Lamella 1, extracted from a Pb-rich dendrite, contains fewer defects.

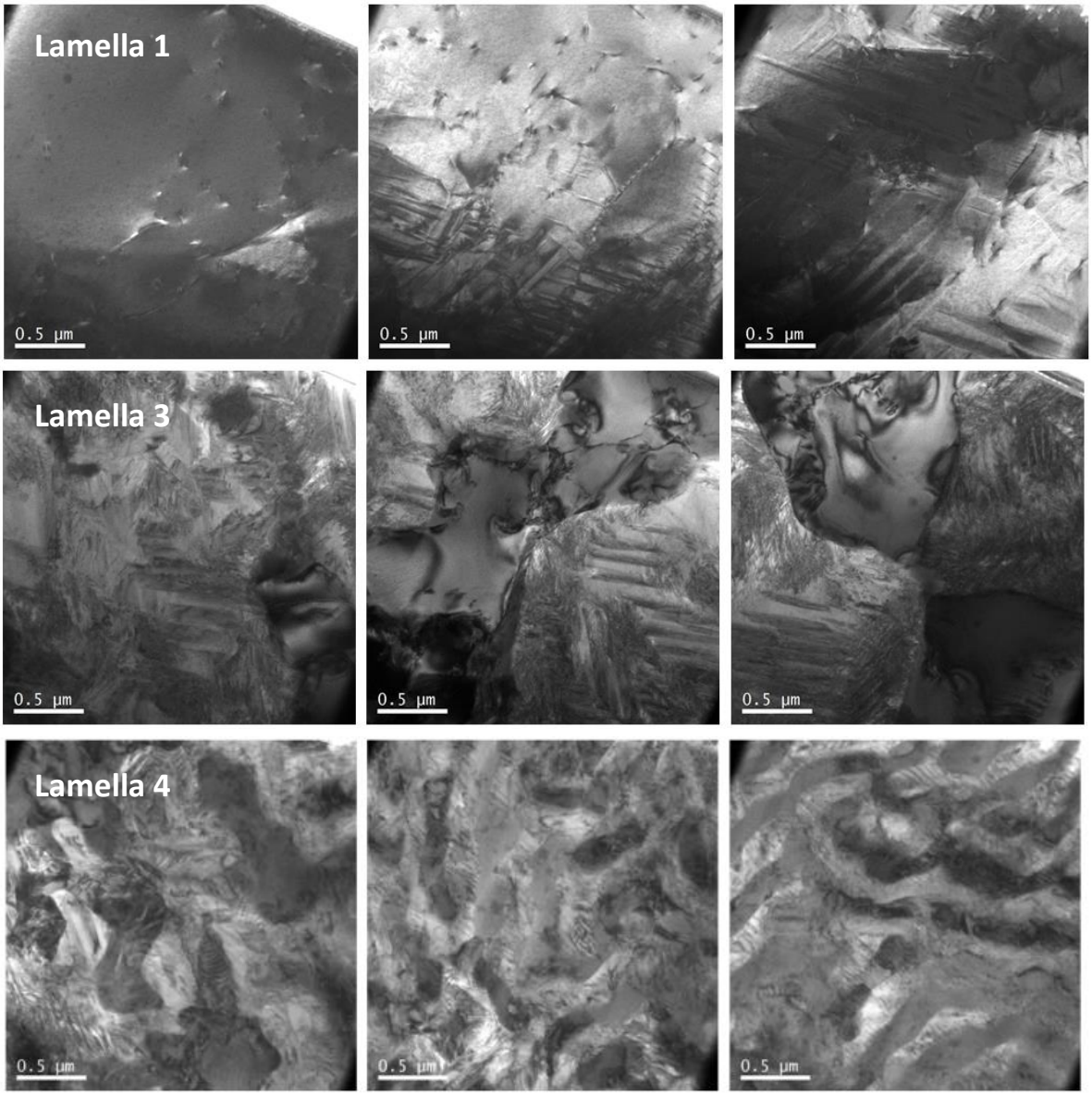

Fig. S5. (a)-(d) STEM images (left) and corresponding EDX elemental maps of the four lamellae extracted from sample A at the locations shown in Fig. 4: Ge (green), Te (blue), Pb (red). (e) Closer view of lamella 4 showing Ge-rich and Pb-rich domain structure.

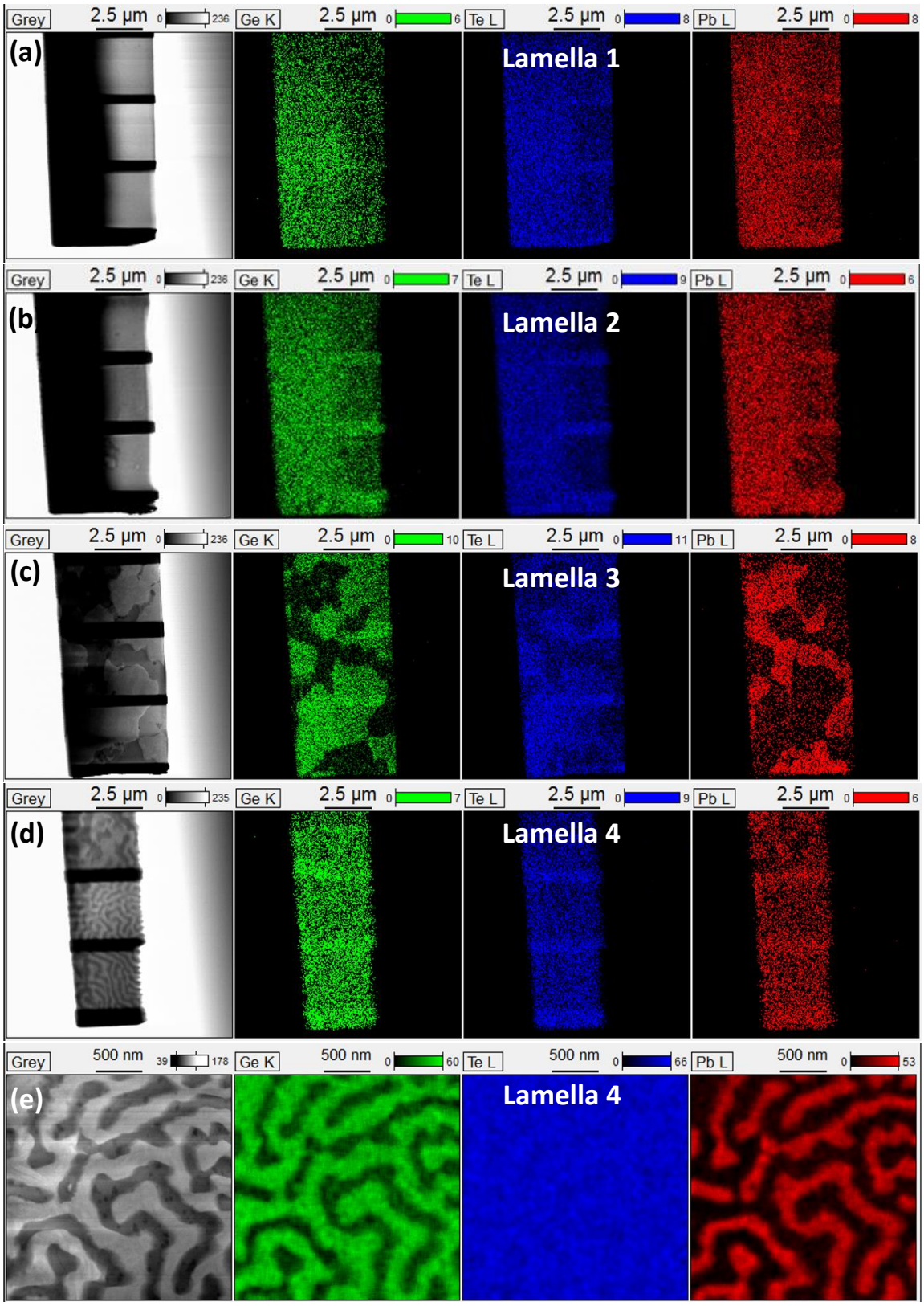

Fig. S6. Temperature dependence of Seebeck coefficient and electrical resistivity of samples A-E measured on warming during (a), (c) initial heating and (b), (d) after twice heating to 400 °C and cooling back to room temperature.

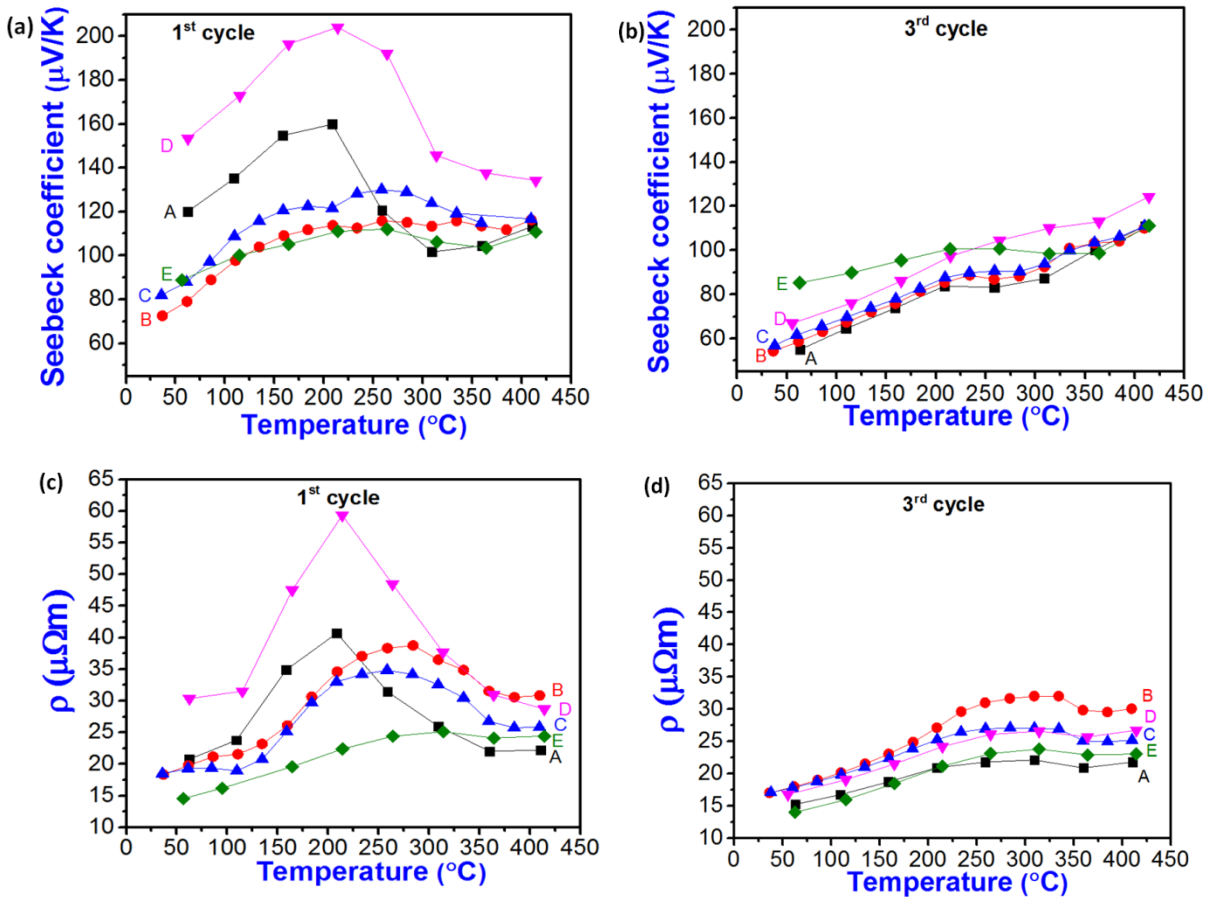

Fig. S7. SEM-BSE images of (a), (b) two representative areas of sample A and (c), (d) two representative areas of sample E, used for estimation of interface density.

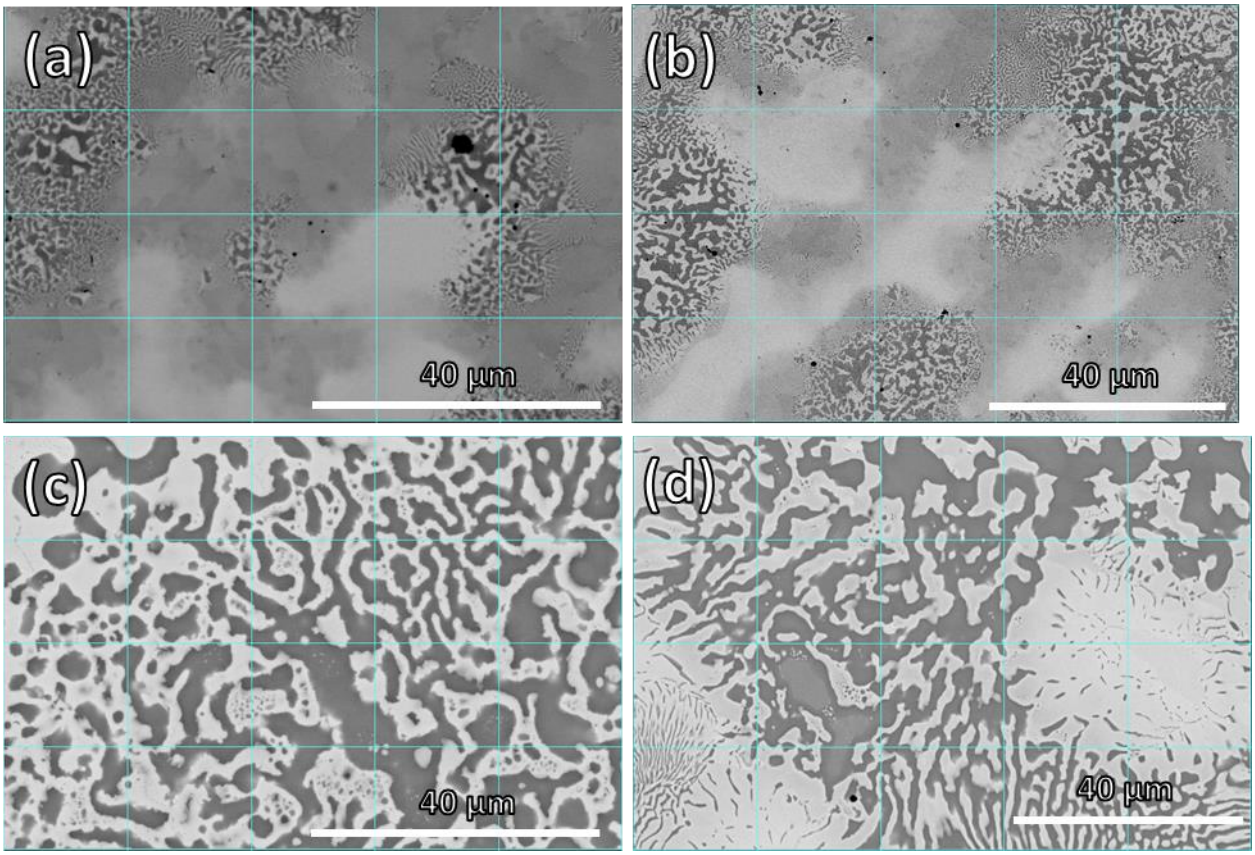

The four SEM-BSE images in Fig. S7 were used to estimate the interface density in samples A and E. This was done by overlaying a grid (blue lines) with total line length L on each image, and manually counting the number of points P at which the grid lines intersect interfaces between light and dark contrast (boundaries between domains of different composition).[1] At the scale of these images, domains of size down to ~0.5 µm can be resolved. The interface density is defined as the surface area of interfaces per unit volume of sample (S_v) in units of mm^{-1} and is estimated by

$$S_V = 2P_L$$

where P_L is the number of points of intersection per unit grid line length. This approach gives an interface density for sample A of 2381 mm^{-1} (Fig. S7a) and 1921 mm^{-1} (Fig. S7b), and an interface density for sample E of 970 mm^{-1} (Fig. S7c) and 806 mm^{-1} (Fig. S7d). The scale of Fig. S7(a) and (c) is the same, and the scale of Fig. S7(b) and (d) is the same. Therefore, we conclude that sample A has a significantly higher density of interfaces than sample E, which will lead to a greater degree of phonon scattering and consequently a lower lattice thermal conductivity, as experimentally observed.

[1] J.C. Russ, *Practical Stereology*, Springer Science and Business Media, New York, 1986.

Fig. S8. Power factor (PF) and figure of merit (ZT) versus temperature measured (a), (c) during initial heating of samples A-E and (b), (d) on heating after two thermal cycles of heating to 400 °C and cooling back to room temperature.